ACS Catalysis

Research Article

pubs.acs.org/acscatalysis

Earth-Abundant Copper-Based Bifunctional Electrocatalyst for Both Catalytic Hydrogen Production and Water Oxidation

Xiang Liu, Huafei Zheng, Zijun Sun, Ali Han, and Pingwu Du*

Key Laboratory of Materials for Energy Conversion, Chinese Academy of Sciences, Department of Materials Science and Engineering, and the Collaborative Innovation Center of Chemistry for Energy Materials (*i*ChEM), University of Science and Technology of China, No. 96 Jinzhai Road, Hefei, Anhui Province 230026, P. R. China

Supporting Information

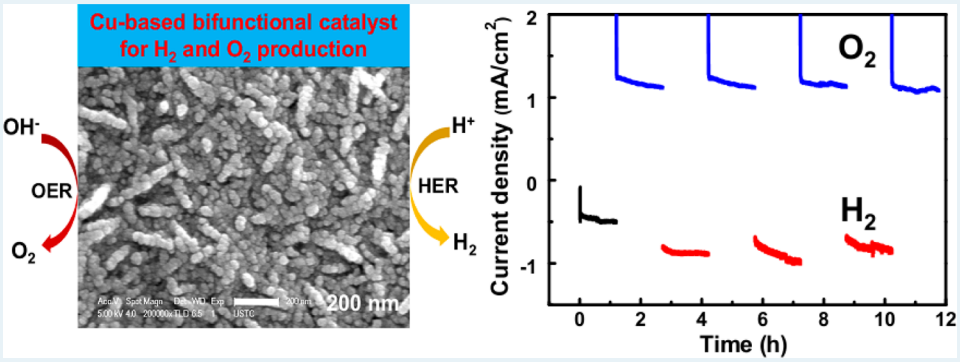

ABSTRACT: The production of hydrogen through water splitting via electrolysis/photocatalysis seems a promising and appealing pathway for clean energy conversion and storage. Herein we report for the first time that a series of water-soluble copper complexes can be used as catalyst precursors to generate the copper-based bifunctional catalyst composite for both hydrogen production and water oxidation reactions. Under an applied cathodic potential, a thin catalyst film was grown on a fluorine-doped tin oxide (FTO) electrode, accompanied by the production of a large amount of hydrogen gas bubbles. Scanning electron microscopy shows the presence of nanoparticulate material on the FTO. Powder X-ray diffraction (XRD) and X-ray photoelectron spectroscopy (XPS) results indicated that the materials consist of amorphous cuprous oxide mixed copper hydroxide (H_2−CuCat), which can catalyze water reduction in a copper-free aqueous solution (pH = 9.2) under a low overpotential. Remarkably, under an applied anodic potential, the material can also efficiently catalyze water oxidation to evolve oxygen. The present robust, bifunctional, switchable, and noble-metal-free catalytic material has potential applications in solar water-splitting devices.

KEYWORDS: *electrocatalysis, noble-metal-free electrocatalyst, copper, water oxidation, hydrogen production, bifunctional*

INTRODUCTION

Hydrogen production by reduction of water has attracted increasing attention because it appears to be an appealing solution for energy storage of renewable energy sources, such as solar energy, if the electric power is obtained through photovoltaics.[1−5] Water splitting can be generally divided into two half-reactions, in which both the hydrogen production reaction and the water oxidation reaction should be catalyzed to expedite multielectron transfer processes and enhance the reaction rates.[3,6−9] Therefore, seeking suitable catalysts seems to be important to develop efficient water-splitting devices for future energy supply plants. However, the catalysts for water splitting are mostly made from the precious metals, such as platinum for hydrogen production,[1,10] and ruthenium[9,11] and iridium[12−15] for water oxidation. Their scarcity and high cost significantly hamper their practicality in applications.

Recently, research has uncovered many abundant and low-cost materials to replace noble metal catalysts for water splitting.[16−18] For the oxidative half-reaction of water splitting, the examples are catalysts based on cobalt,[19−24] nickel,[25−28] and iron.[29,30] The cobalt-based materials generally show higher catalytic activity than other first-row transition metals-based materials. The representative examples include the cobalt-phosphate (Co-Pi) catalyst,[19,31,32] cobalt polyoxometalate (Co-POM),[33,34] and Co_3O_4 catalyst.[35,36] For the reductive half-reaction, the examples are catalysts based on molybdenum, nickel, and cobalt.[37−39] Du Bois et al. reported a series of Ni-based molecular catalysts, in which the highest reaction turnover frequency has reached as high as 100 000 s^{-1}.[40] More recently, cobalt-based and nickel-based heterogeneous catalysts have exhibited remarkable Janus properties to catalyze both hydrogen production and water oxidation reactions in the

Received: September 28, 2014
Revised: January 23, 2015
Published: January 26, 2015

DOI: 10.1021/cs501480s
ACS Catal. 2015, 5, 1530−1538

same reaction electrolyte when the applied potentials are switched between oxidative conditions and reductive conditions.[41−43] This switch is fully reversible and stable during catalysis. These findings provide new possibilities with respect to electrodeposition of the electrocatalyst for both hydrogen production and water oxidation reactions using the same catalyst precursor in one buffered solution. Despite this reported progress, there are still substantial challenges in developing highly efficient, stable, and low-cost catalysts for water splitting.

Compared with cobalt, nickel, and molybdenum, copper (Cu) is more attractive because of its much higher abundance and lower price. Copper plays a key role as the metal center in the respiratory enzyme complex cytochrome C oxidase and other enzymes, which are essential to living organisms. The reduction of Cu^{II} to Cu^{I}/Cu^{0} and oxidation to Cu^{III}/Cu^{IV} provides Cu^{II} with well-defined coordination chemistry and extensive redox properties.[44−48] The high abundance, low toxicity, and rich redox properties render Cu-based catalysts highly favorable for possible energy applications. In earlier studies, several copper complexes have been reported to be active as homogeneous catalysts for water oxidation[49−53] and hydrogen production.[54,55] Cu^{0} nanoparticles have also been studied for CO_2 reduction.[56] Recently, our group reported on the use of copper(II) tris(2-pyridylmethyl)amine complexes as catalyst precursors to deposit heterogeneous copper-oxide-based film on conductive electrode for water oxidation.[57]

In this present study, we demonstrate that copper complexes **1**−**4** (Scheme 1) can promote hydrogen production in a nearly

Scheme 1. Molecular Structures of Copper(II) Complexes

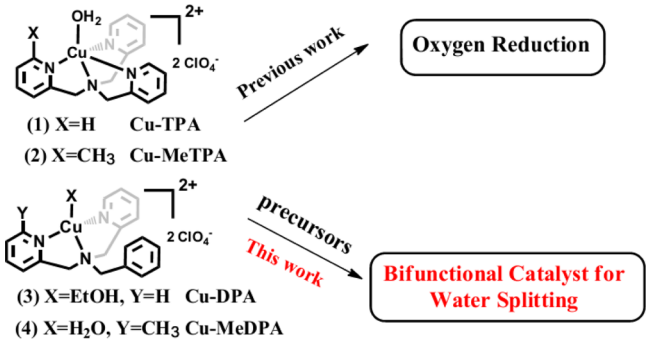

neutral aqueous solution (pH = 9.2) at low overpotentials and exhibit good stability. The electrodeposited material (H_2−CuCat) under a cathodic potential can be easily used as the water oxidation catalyst (O_2−CuCat) to catalyze oxygen evolution under oxidative conditions. The switch between these two catalytic forms is fully reversible. The catalyst films were extensively studied by scanning electron microscopy (SEM), energy-dispersive X-ray analysis (EDX), X-ray photoelectron spectroscopy (XPS), and powder X-ray diffraction (XRD).

RESULTS AND DISCUSSION

Electrocatalytic H_2 Production. Figure 1a shows the cyclic voltammograms (CVs) of four copper complexes (**Cu-TPA**, **Cu-MeTPA**, **Cu-MeDPA**, **Cu-DPA**, 0.68 mM), and one simple $CuCl_2$ salt (0.68 mM) in a 0.1 M potassium borate (KBi) solution at pH 9.2 using FTO as the working electrode, an Ag/AgCl (3 M KCl) electrode as the reference electrode, and Pt wire as the counter electrode. The CVs data show that all of these copper complexes are active for the reductive half-reaction of water splitting during cathodic scans from 0 V to −1.50 V (all the potentials in this paper are versus Ag/AgCl). **Cu-TPA** and **Cu-MeTPA** show much higher catalytic current densities than the other three copper complexes. For **Cu-TPA**, the onset of a sharp catalytic wave is observed at −1.20 V (overpotential, ∼0.45 V), accompanied by gas bubbles emerging on the surface of FTO. The gas bubbles were confirmed to be hydrogen by gas chromatography (GC). The cathodic scan also exhibits a broad feature at $E_{p,c}$ = −0.50 V, attributed to the reduction of the starting material of the copper complex. Performing the same cyclic voltammograms experiment but using glassy carbon electrode (GC) as the working electrode confirmed the presence of a reductive peak at around −0.50 V (Figure 1a, inset). The results indicate that this peak should be assigned to Cu(II)/Cu(I) instead of reducing Sn element on FTO.[58] The black plot in Figure 1a is the control experiment containing no catalyst and operating at pH 9.2, which showed no appreciable catalytic current, indicating that the existence of copper complexes are essential to the observed catalytic reaction.

To provide more insights into the hydrogen evolution reaction catalyzed by **Cu-TPA**, bulk electrolysis experiments were carried out in a 0.1 M KBi electrolyte at −1.10 V, −1.20 V, and −1.30 V (Figure 1b). Thin brown-colored films were electrodeposited on the surface of the FTO and large amounts of hydrogen gas bubbles were produced on the working electrode for the applied potentials of −1.20 V and −1.30 V. As a higher potential was applied, higher catalytic current density was obtained. During bulk electrolysis, the current density reaches a plateau at 0.75 mA/cm^2 and 1.4 mA/cm^2 for the applied potential of −1.20 V and −1.30 V, respectively, as shown in Figure 1b. The catalyst film was then transferred to a clean KBi solution containing no **Cu-TPA**. A nearly identical current density is achieved under the same applied potential, as shown in Figure 1c. This result indicates that the electrodeposited film is the real active catalyst toward the water reduction reaction to produce hydrogen. We named this electrodeposited material H_2−CuCat. Similar results are also obtained in a 0.1 M potassium phosphate (KPi) buffer solution at pH 7.0, as shown in Figure S1. The catalytic current densities for hydrogen production are highly dependent on pH values, as shown in Figure 1d. Higher catalytic current intensities were achieved when the pH values decreased from pH 7.0 to 1.0, which is consistent with the thermodynamic tendency for water reduction. The black dash plot in Figure 1d is the control experiment containing no copper complex operated at pH 7.0, showing no appreciable catalytic wave.

Bulk electrolysis experiments (BE) were also carried out in a 0.1 M KBi electrolyte containing **Cu-MeTPA**, **Cu-MeDPA**, **Cu-DPA**, and $CuCl_2$ with an applied cathodic potential at −1.20 V (Figure S2). Similar brown thin films were observed on the FTO electrodes during bulk electrolysis. Consistent with the CVs data, the BE results show that **Cu-TPA** and **Cu-MeTPA** achieved much higher catalytic activities. For example, **Cu-MeDPA** and **Cu-DPA** achieve obvious catalytic current densities of less than ∼0.3 mA/cm^2 with an applied cathodic potential at −1.20 V. In contrast, **Cu-TPA** and **Cu-MeTPA** could achieve more than −0.60 mA/cm^2 under the same conditions. The above results indicate that the organic ligands in these copper complexes may play an important role in water reduction for hydrogen production. However, the real roles of

DOI: 10.1021/cs501480s
ACS Catal. 2015, 5, 1530−1538

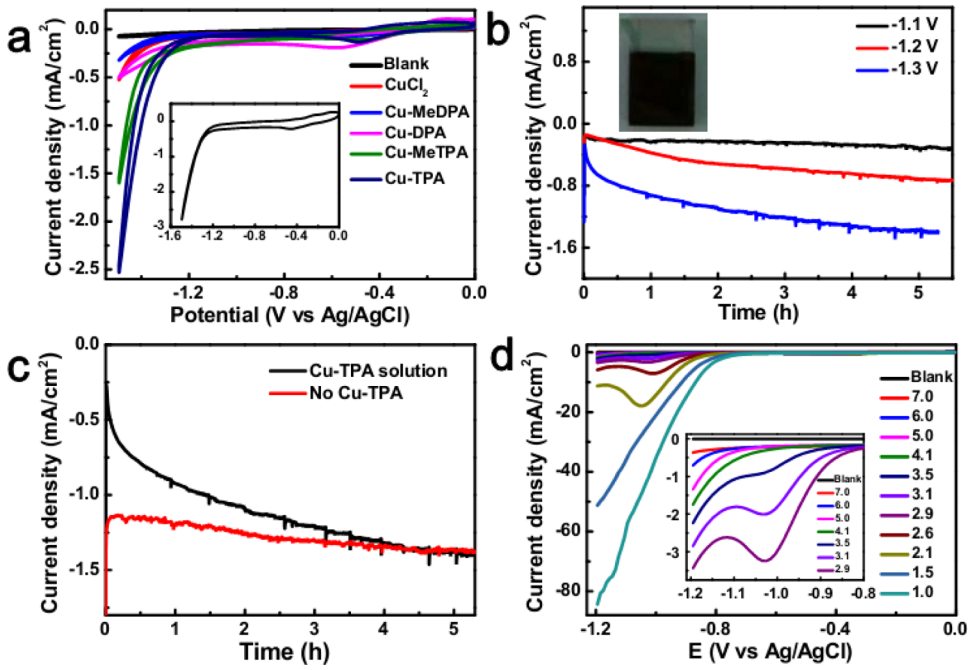

Figure 1. (a) CVs in a 0.1 M KBi solution using FTO electrode as the working electrode under pH 9.2 in the presence of 0.68 mM $CuCl_2$ (red), **Cu-MeDPA** (blue), **Cu-DPA** (pink), **Cu-MeTPA** (green), and **Cu-TPA** (navy). Inset: CV scan in the **Cu-TPA** solution using GC electrode. (b) Current density plot for bulk electrolysis at −1.10 V (black), −1.20 V (red), and −1.30 V (blue) in 0.1 M Bi electrolyte, 0.68 mM **Cu-TPA**, pH 9.2 using a FTO cathode. Inset: the photo of the H_2−CuCat film obtained from **Cu-TPA**. (c) The profiles of bulk electrolysis obtained in a 0.1 M Bi solution, pH 9.2 using a FTO cathode containing 0.68 mM **Cu-TPA** using a bare FTO working electrode (black plot) and containing no Cu-TPA using the H_2−CuCat thin film (red plot). (d) CVs with 0.68 mM **Cu-TPA** in a 0.1 M KPi solution using GC electrode as the working electrode under different pH. The scan rate is 50 mV/s and there is *iR* compensation (∼3−5 Ω) for CVs.

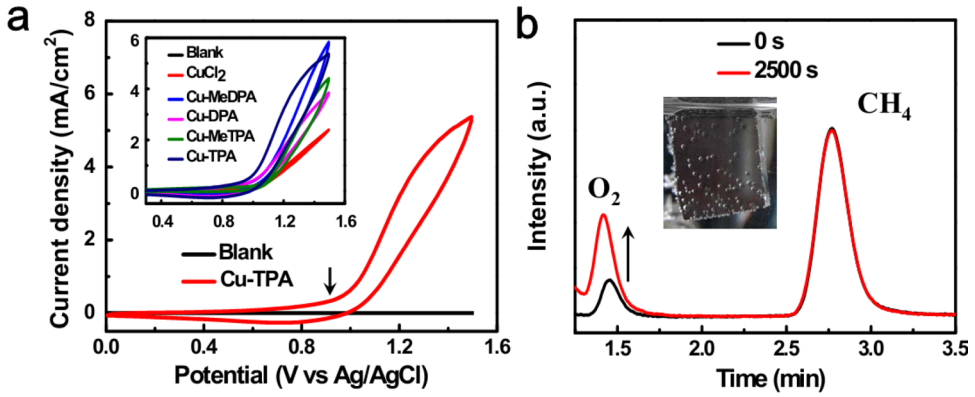

Figure 2. (a) CVs in a 0.1 M KBi solution at pH 9.2 using a clean FTO plate (black) and electrodeposited H_2−CuCat film (red) obtained from **Cu-TPA** as the working electrodes. Inset: CVs using the electrodeposited H_2−CuCat catalyst films obtained from 0.68 mM $CuCl_2$ (red), **Cu-MeDPA** (blue), **Cu-MeTPA** (green), and **Cu-TPA** (navy) in a 0.1 M KBi solution at pH 9.2. The scan rate is 50 mV/s and there is *iR* compensation (∼3−5 Ω) for CVs. (b) Gas chromatographic traces in the presence of O_2−CuCat modified FTO obtained from **Cu-TPA** after electrolysis for 0 s (black) and 2500 s (red) at 1.10 V vs Ag/AgCl. The chromatographic response for O_2 is referenced to methane peak (CH_4).

these ligands are unclear due to the difficulty to track the reaction intermediates. The catalytic difference may result from the different morphologies of the electrodeposited catalyst films, as discussed in the following SEM part.

Electrocatalytic Water Oxidation. More interestingly, we found that the electrodeposited thin films can also catalyze water oxidation reaction (Figure 2). After the H_2−CuCat thin film was generated by a few hours of electrodeposition, the electrode was transferred to a 0.1 M KBi solution (pH = 9.2) and the applied potential was switched to the oxidative conditions. Figure 2a shows the CVs data using the H_2−CuCat catalyst electrodeposited from **Cu-TPA** as the working electrode. An obvious catalytic current is clearly observed during CV scans from 0 to 1.50 V for **Cu-TPA** precursor, accompanied by gas bubbles emerging on the working electrode. When the working electrode was replaced by other H_2−CuCat materials electrodeposited from **Cu-MeTPA**, **Cu-DPA**, **Cu-MeDPA**, and $CuCl_2$ precursors, the CVs data showed that all these four H_2−CuCat materials were catalytically active for water oxidation (Figure 2a, inset). The black line is the control experiment using bare FTO as the working electrode in a clean KBi solution (pH = 9.2), showing no appreciable catalytic current from 0 to 1.50 V.

DOI: 10.1021/cs501480s
ACS Catal. 2015, 5, 1530−1538

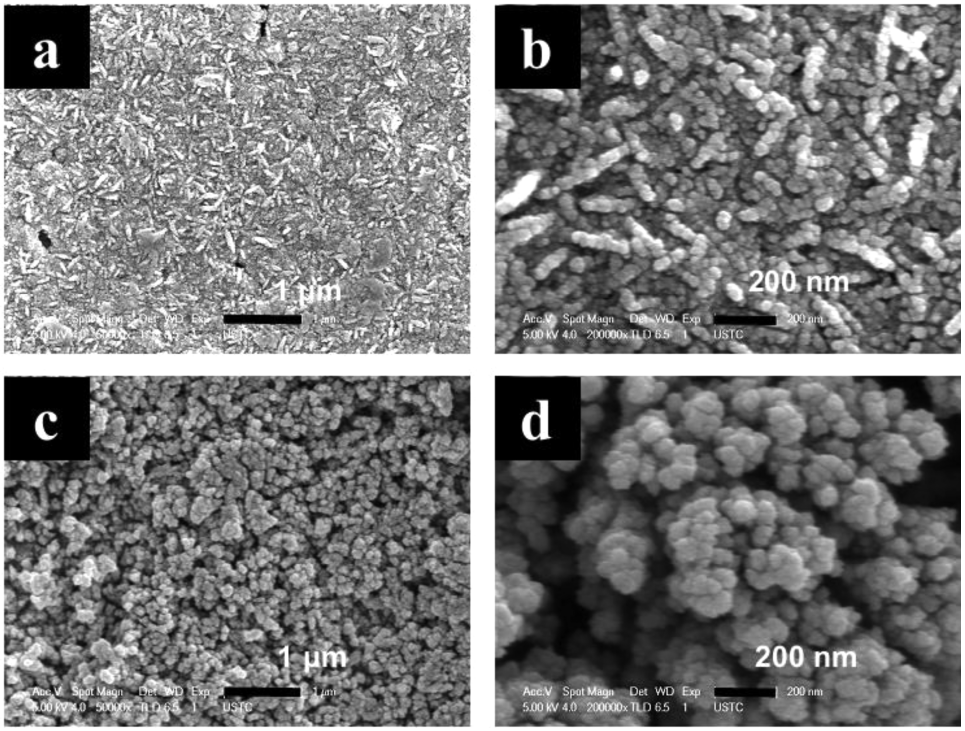

Figure 3. Scanning electron microscopy (SEM) images of H_2−CuCat catalyst electrodeposited on the FTO surface prepared by bulk electrolysis at −1.20 V for 10 h in a 0.1 M KBi buffer solution at pH 9.2 containing 0.68 mM **Cu-TPA** (a and b). The O_2−CuCat obtained from the above H_2−CuCat after redox switch to +1.10 V for 10 h (c and d).

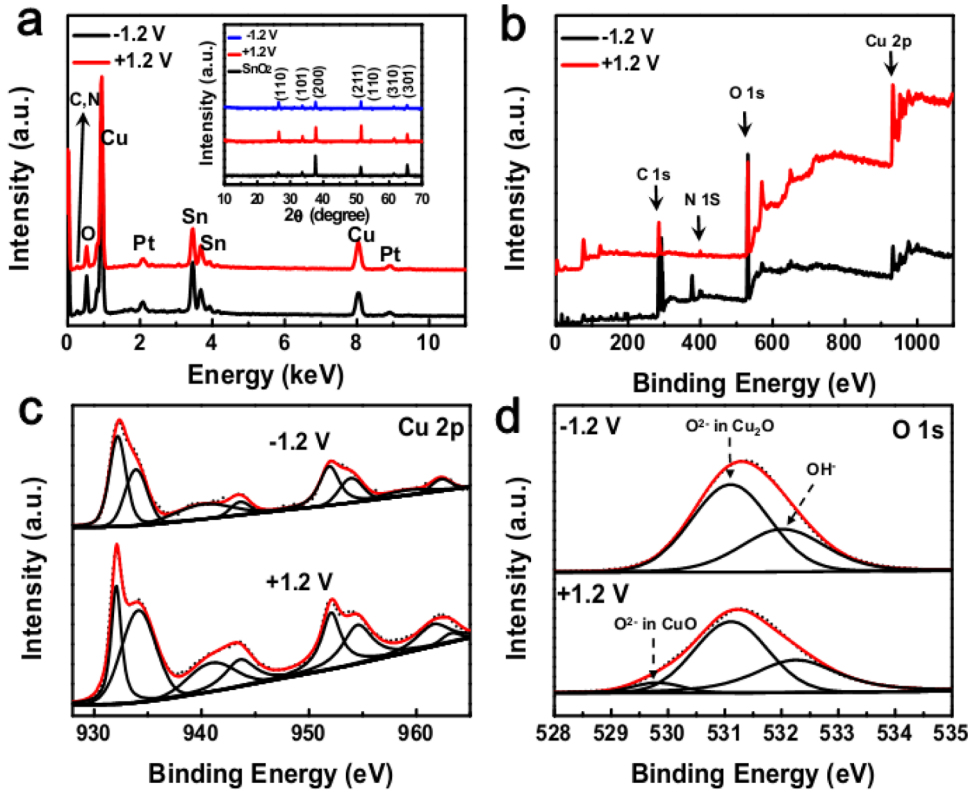

Figure 4. (a) EDX spectra of the electrodeposited H_2−CuCat film on FTO electrode (black) and the O_2−CuCat film (red) obtained from **Cu-TPA**. Inset: XRD data of the H_2−CuCat (black), O_2−CuCat (red), and the clean FTO (blue). (b) X-ray photoelectron spectroscopy (XPS) survey data of the H_2−CuCat catalyst (black) and the O_2−CuCat catalyst (red). (c) The high-resolution XPS spectra of Cu 2p region of the H_2−CuCat catalyst (top) and the O_2−CuCat catalyst (bottom). (d) The high-resolution XPS spectra of O 1s region of the H_2−CuCat catalyst (top) and the O_2−CuCat catalyst (bottom).

DOI: 10.1021/cs501480s
ACS Catal. 2015, 5, 1530−1538

In addition, bulk electrolysis experiments of the electrodeposited H_2−CuCat modified FTO electrodes under anodic potential are shown in Figure S3. A quite low applied anodic potential at +1.10 V result in catalytic current densities of >0.30 mA/cm^2. Obvious gas bubbles were observed on the working electrode, which were confirmed to be oxygen by a fluorescence-based oxygen sensor and gas chromatography (GC). After an electrolysis period of 2500 s, the volume of the oxygen gas had clearly increased (Figure 2b) and the CH_4 gas as the reference stayed the same, confirming the production of oxygen. We named these materials for water oxidation O_2−CuCat.

SEM Images. Figure 3 is the scanning electronic micrographs (SEM) of the electrodeposited materials H_2−CuCat and O_2−CuCat using **Cu-TPA** as the catalyst precursor in a 0.1 M KBi solution at pH 9.2. Isolated nanoparticles with an average diameter of ∼20 nm were observed on the H_2−CuCat catalyst film electrodeposited from **Cu-TPA** (Figure 3a,b). Under oxidative conditions, the H_2−CuCat catalyst was converted to more uniform nanoparticles with a larger diameter (∼35 nm, Figure 3c,d), indicating the O_2−CuCat film has different morphology from H_2−CuCat. Performing the same electrolysis but using **Cu-MeTPA** as the catalyst precursor yields a catalyst film made from small nanoparticles (∼10 nm) with some big islands (Figure S4a). However, the corresponding O_2−CuCat film under an anodic potential shows very loose morphology with larger size in diameter (100−150 nm, Figure S4b). Figure S4c,d are the SEM images of a catalyst film made from a $CuCl_2$ solution, which shows less uniform morphology than the catalyst films made of **Cu-TPA** and **Cu-MeTPA** precursors. This may be one of the reasons for that its catalytic activity toward water reduction reaction is obviously lower than the other two catalysts.

Physical Characterization. Subsequently, the catalyst materials electrodeposited under the reductive and oxidative conditions were further characterized by EDX and powder XRD. The EDX results (Figure 4a) suggest that the main elements in H_2−CuCat and O_2−CuCat materials are Cu and O. In addition, the Sn signal probably arises from the FTO substrate. Pt is artificially sprayed on the surface of the film to increase the conductivity. The powder XRD data acquired from these two catalytic films reveal the amorphous features and no peaks related to crystalline phases of copper/copper oxide were observed except those patterns associated with the FTO substrate (Figure 4a, inset).

The X-ray photoelectron spectroscopy (XPS) was used to probe the chemical states of freshly electrodeposited films (Figure 4b−d). The XPS survey revealed both catalyst films mainly contain Cu, O, and Sn elements (Figure 4b), which is consistent with the results observed from the EDX spectra. The C 1s peak (285.0 eV) was used as the reference. Figure 4c shows the high-resolution XPS spectra of Cu 2p. In the Cu 2p spectra, obvious shakeup satellite peaks were observed, which is a typical characteristic of Cu-based materials.[59,60] The Cu 2p spectra of both H_2−CuCat and O_2−CuCat film exhibited similar shape and peaks. The binding energies of Cu $2p_{3/2}$ can be fitted well by two peaks located at 932.4 and 933.9 eV, and the binding energies of Cu $2p_{1/2}$ show two peaks located at 952.2 and 954.0 eV. Cu $2p_{1/2}$ binding energy at 952.2 eV and the Cu $2p_{3/2}$ binding energy at 932.4 eV indicate the existence of Cu_2O.[61−63] The presence of Cu_2O could be further confirmed by the O 1s binding energy at 531.0 eV (Figure 4d).[62] The existence of $Cu(OH)_2$ were also possible, as evidenced by the binding energy of Cu $2p_{3/2}$ located at 933.9 eV.[62,64] An intense peak at 532.1 eV in O 1s can be assigned to $Cu(OH)_2$.[62] Because the Cu(0) owns similar binding energy location to Cu_2O in Cu 2p spectra and the catalytic H_2−CuCat material exhibits slight metallic luster after long-term electrolysis (>10 h), it is possible that H_2−CuCat material contains some Cu(0). In order to avoid the influence of Cu(0), bulk electrolysis was performed for less than 6 h and the color of this deposited H_2−CuCat film did not show any metallic luster by naked eyes. In addition, the absence of O^{2-} at 529.6 eV excludes the presence of CuO in the H_2−CuCat. Therefore, H_2−CuCat material is possibly composed of Cu_2O and $Cu(OH)_2$, and some Cu(0).

The XPS spectra of O_2−CuCat show appreciable differences from H_2−CuCat. First, the ratio of Cu $2p_{3/2}$ binding energies located at 933.9 and 932.4 eV becomes bigger in O_2−CuCat, indicating the component at 933.9 eV increases. Second, a new binding peak at 529.6 eV appears in O 1s spectrum, which is the typical peak of the O^{2-} in CuO.[62,63] The presence of CuO can be further confirmed by the presence of a new peak at 917.8 eV from the $CuLM_2$ spectrum (Figure S5). The peak located at 915.8 eV remains nearly the same position, indicating the presence of Cu_2O and $Cu(OH)_2$.[63,65] The above results show CuO may result from the oxidation of Cu_2O or decomposition of $Cu(OH)_2$. Previous XPS studies of transition metal surface oxidation suggested that chemisorbed water[66] and chemisorbed hydroxyl oxygen species[67] contributed to the peaks at around 532.4 and 531.2 eV. The content of CuO reflected from O 1s spectrum is not as accurate as Cu LM_2 spectrum. Therefore, the ratio of Cu_2O, $Cu(OH)_2$, and CuO in the O_2−CuCat film can be calculated from the Cu 2p and Cu LM_2 XPS spectra. From the XPS results, the ratio of Cu_2O and $Cu(OH)_2$ on the surface of H_2−CuCat film is around 1.0:1.5. As for the surface of O_2−CuCat film, the ratio of Cu_2O, $Cu(OH)_2$, and CuO is around 1.0:1.0:3.0.

In addition, the H_2−CuCat catalyst film electrodeposited from **Cu-TPA** in a KPi buffered solution (pH = 7.0) shows very similar nanoparticles to that obtained in KBi, with an average diameter of ∼20 nm (Figure S6a). The nanoparticulate catalyst film has the same composition as the H_2−CuCat material obtained in a KBi buffered solution at pH = 9.2. XPS data also show the material contains CuO, $Cu(OH)_2$, and some Cu(0) component (Figure S6b and Figure S7). Furthermore, XRD results show that the nanoparticles is amorphous and only FTO substrate peaks could be observed (Figure S8).

Faraday Efficiency and the Tafel Plot. Under the reductive conditions, quantitative hydrogen production experiments were performed in a gastight electrochemical cell with the H_2−CuCat film coated FTO as the working electrode (Figure 5a). When a cathodic potential of −1.20 V was applied, hydrogen bubbles were rapidly produced on the working electrode. The amount of hydrogen gas was measured by gas chromatography. A plot for hydrogen production was obtained as a function of operation time. The theoretical amount of hydrogen under the applied potential of −1.20 V was calculated by assuming that all charges that passed through the working electrode were from 2e$^-$ reduction of protons by Faraday's Law. The amount of hydrogen generation during bulk electrolysis matched well with the theoretical amount of hydrogen, corresponding to an efficiency of nearly 100% in 2 h. Furthermore, the Faradaic efficiency of the O_2−CuCat electrocatalyst was measured by a fluorescence-based oxygen sensor (Figure 5b). Bulk electrolysis was performed in a 0.1 M

DOI: 10.1021/cs501480s
ACS Catal. 2015, 5, 1530−1538

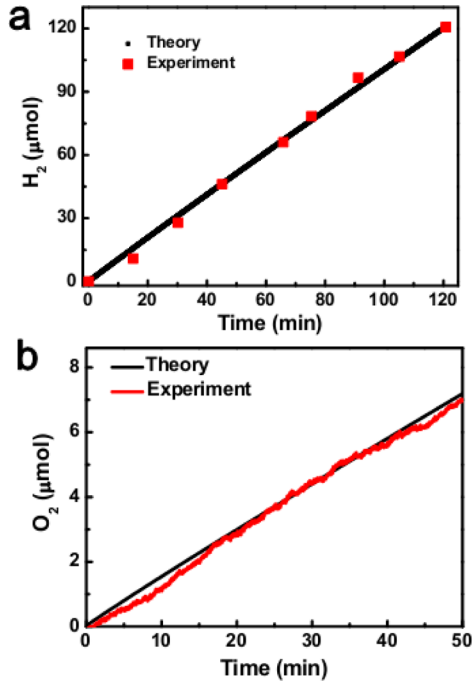

Figure 5. (a) Theoretical and experimental hydrogen evolution from water by bulk electrolysis at −1.20 V using the electrodeposited H_2−CuCat catalyst. (b) Theoretical and experimental oxygen evolution from water by bulk electrolysis at +1.20 V using the O_2−CuCat catalyst obtained from Cu-TPA at pH 9.2 in a 0.1 M KBi electrolyte.

KBi solution at pH 9.2 in a gastight electrochemical cell with an applied anodic potential of +1.20 V. After the electrolysis was initiated, a significant amount of oxygen bubbles was produced on the working electrode and the fluorescence-based oxygen sensor showed the rise of the oxygen percentage in the headspace. The theoretical amount of oxygen evolution under the applied potential +1.20 V was calculated by assuming that the total charge was from $4e^-$ oxidation of water by Faraday's law. The amount of produced oxygen matched well with the theoretical amount of oxygen, corresponding to a Faradaic efficiency of ∼97% in 50 min (Figure 5b). The result shows that the O_2−CuCat electrocatalyst is highly active for water oxidation to produce oxygen.

To further study the electrocatalytic properties of the H_2−CuCat and O_2−CuCat materials, the Tafel plots were obtained by measuring the stable current density (j) of these H_2−CuCat and O_2−CuCat catalyst films at various potentials as a function of the overpotential (η) based on the Nernstian potential for water reduction or water oxidation in a 0.1 M KBi solution (pH 9.2) (Figure S9 and Figure 6). The overpotential is defined as $\eta = V_{appl} - iR - E_{pH}$, V_{appl} is the applied potential vs NHE, i is the stable current, R is the uncompensated resistance, and E_{pH} is the thermodynamic potential for water reduction/oxidation at this pH (for water reduction, $E_{pH} = -0.059$ pH V vs NHE; for water oxidation, $E_{pH} = 1.23$ V − 0.059 pH V vs NHE). Figure S9 is the Tafel plot of the H_2−CuCat material and a current density of 1.0 mA/cm^2 requires an overpotential of 440 mV. However, a relatively high Tafel slope of 320 mV/dec was obtained, indicating a complicated process. The high slope not only demonstrates the catalytic properties of the catalyst film but also shows the reduction of copper species, as evidenced by the appearance of a reduction peak at an overpotential of ∼−0.16 V (∼−0.50 V vs Ag/AgCl, which is consistent with

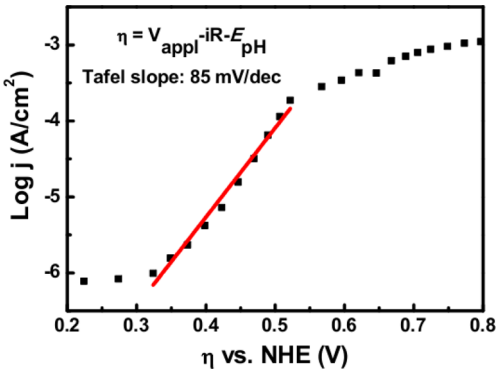

Figure 6. Tafel plot, $\eta = V_{appl} - iR - E_{pH}$, of the O_2−CuCat film obtained from **Cu-TPA** in a 0.1 M KBi solution at pH 9.2.

Figure 1a, inset). Figure 6 is the Tafel plot of the O_2−CuCat material and appreciable catalytic current is observed when η = 0.33 V. Consistent with the Tafel slope, the onset potential in Figure 2a was located at ∼0.8 V, indicating the overpotential was located at ∼0.32 V and the current density can reach to 0.18 mA/cm^2. Such a value of η is comparable to the catalytic activity of Co-Pi (η = 0.28 V) and Ni−Bi (η = 0.31 V) catalysts reported in the literature.[19,26] A nearly linear relationship with the slope of the line as ∼85 mV/decade was observed from 0.32 to 0.52 V.

Bifunctional Performance for H_2 Production and Water Oxidation. Finally, the H_2−CuCat catalyst film electrodeposited at −1.20 V from **Cu-TPA** was used for both hydrogen production reaction and water oxidation reaction in the same electrochemical cell (Figure 7). The H_2−CuCat

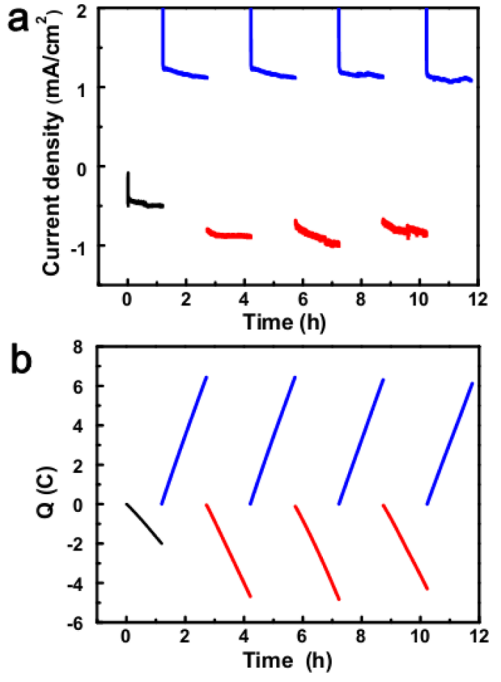

Figure 7. (a) Current−time plot for FTO electrode during controlled potential coulometry initially at −1.20 V (1.5 h, H_2−Cat deposition, black lines) in 0.1 M Bi electrolyte (pH = 9.2) containing 0.68 mM **Cu-TPA**. Then, the film was transferred into a clean KBi solution, with the potential switched between oxidative (+1.20 V, blue lines) and reductive conditions (−1.20 V, red lines). (b) Charges passed through the FTO electrode during the same experiment.

DOI: 10.1021/cs501480s
ACS Catal. 2015, 5, 1530−1538

catalyst film was grown under a cathodic potential at −1.20 V for 1.5 h (1 C charges were passed through the working electrode) and then transferred into a 0.1 M copper-free KBi solution (pH = 9.2). After 1.5 h of bulk electrolysis at +1.20 V, the potential was switched to the reductive conditions (−1.20 V). The alternating switching was continuously performed between oxidative and reductive conditions (Figure 7a,b) in the same solution. During these switching experiments, appreciable gas bubbles were clearly observed on the working electrode, which was confirmed to be O_2 and H_2, respectively. The stable current density was about −1.0 mA/cm^2 at the −1.20 V for hydrogen reduction and +1.10 mA/cm^2 at +1.20 V for water oxidation. The switch between hydrogen production and water oxidation shows good reversibility. The results demonstrate that the H_2−CuCat/O_2−CuCat catalyst film is highly efficient for both hydrogen production reaction and water oxidation reaction, and the film has good stability during bulk electrolysis for water splitting.

Mechanism of Electrodeposition and Catalytic Water Splitting. Cathodic electrodeposition in a solution containing simple Cu salts usually results in the generation of Cu(0) under a high potential.[56] The CV scan in a $CuCl_2$ solution shows negligible catalytic current at 0−1.5 V, as shown in Figure 1a, indicating Cu(0) deposited from Cu^{2+} did not play an important role for H_2 production. This may be because that most of Cu^{2+} ions are precipitated at pH 9.2. Based on the XPS results, Cu_2O and $Cu(OH)_2$ are the major electrodeposited components instead of Cu(0). As previously reported,[68] ligand-mediated reduction of the metal from Cu^{2+} to Cu^+ and from Cu^+ to Cu^0 can occur under certain conditions. The **TPA** ligand in **Cu-TPA** might also control the generation of Cu^+ (eq 1), as evidenced by the small reduction peak at around −0.50 V in Figure 1a. Under basic conditions, Cu^+ may rapidly react with OH^- to form CuOH (eq 2), which is not stable and can be decomposed to produce Cu_2O (eq 3) or oxidized by the dissolved oxygen to produce $Cu(OH)_2$ (eq 4) on the electrode. Precipitation of Cu_2O may be also due to the limited solubility of Cu^+ ions in water (eq 5).[58] Because both Cu_2O and $Cu(OH)_2$ can promote H_2 production reaction,[69−71] it is reasonable to conclude that these two species probably are the real catalysts in H_2−CuCat.

Under oxidative potentials, the H_2−CuCat material was converted to O_2−CuCat. The XPS results indicated that the O_2−CuCat was composed of Cu_2O, $Cu(OH)_2$, and a little bit CuO. As discussed above, part of Cu_2O in H_2−CuCat could be oxidized to produce CuO. CuO has been recently reported as an active catalyst toward water oxidation reaction.[57] We further examined the catalytic activity of commercial Cu_2O and $Cu(OH)_2$ for water oxidation. The CV results show that both Cu_2O and $Cu(OH)_2$ can catalyze water oxidation reaction and promote catalytic current density accompanied by obvious oxygen gas bubbles (Figure S10). Therefore, in the presence of CuO, Cu_2O and $Cu(OH)_2$, the O_2−CuCat film is highly active toward water oxidation. It is worthwhile to mention that the ratio of CuO in the O_2−CuCat is very small and the major compositions are Cu_2O and $Cu(OH)_2$. Overall, Cu_2O and $Cu(OH)_2$ in H_2−CuCat and O_2−CuCat films probably play important roles for both hydrogen production and water oxidation reactions.

$$\mathrm{Cu - TPA} \xrightarrow{+e^-} \mathrm{Cu^+ + TPA} \quad (1)$$

$$\mathrm{Cu^+ + OH^- \rightarrow CuOH} \quad (2)$$

$$\mathrm{2CuOH \rightarrow H_2O + Cu_2O} \quad (3)$$

$$\mathrm{4CuOH + O_2 + 2H_2O \rightarrow 4Cu(OH)_2} \quad (4)$$

$$\mathrm{2Cu^+ + H_2O \rightarrow Cu_2O + 2H^+} \quad (5)$$

The present copper(II) complexes have some advantages over simple divalent copper salts to electrodeposit the above-mentioned H_2−CuCat catalyst for bifunctional performance. Previous study has reported that simple divalent copper salts can be used to electrodeposit Cu(0) films on conductive electrode under negative potentials in 0.1 M $NaHCO_3$ (pH ∼ 6.7),[56] but the catalyst film did not contain $CuO_x/Cu(OH)_2$, which can catalyze the water oxidation reaction. Meanwhile, although aqueous solutions of other simple Cu^{2+} salts, such as $CuSO_4$ and $Cu(OAc)_2$ have been used to electrodeposit Cu_2O films to construct photoelectrochemical cells,[72−74] there are no methods reported in the literature to obtain a copper-based bifunctional electrocatalyst for water splitting. In our present study, simple divalent $CuCl_2$ in a KBi solution (pH = 9.2) did not show good catalytic activity for hydrogen production (Figure 1a). On the other hand, divalent copper salts will be easily precipitated to generate $Cu(OH)_2$ in a 0.1 M KBi buffer solution at pH 9.2, resulting in a very low concentration of Cu^{2+} ions in solution. The results showed that the catalyst film electrodeposited from $CuCl_2$ was far less active than the H_2−CuCat films deposited from **Cu-TPA** and **Cu-MeTPA** for the hydrogen production reaction.

CONCLUSIONS

In summary, a series of water-soluble copper complexes were used as the catalyst precursors to generate bifunctional H_2−CuCat catalyst film for both hydrogen production and water oxidation reactions. The H_2−CuCat catalyst is remarkable for the following reasons. First, it is easily prepared by simple electrodeposition from organic copper pyridyl−methylamine complexes. Second, the H_2−CuCat catalyst is robust and active for water reduction to produce hydrogen at a low overpotential (∼0.45 V, calculated at −1.20 V) under weak basic conditions at pH 9.2. Third, it can be used as water oxidation catalyst (O_2−CuCat) for oxygen evolution with appreciable catalytic current at η = 0.33 V. The switch between the two catalytic forms was fully reversible. After electrodeposition, the catalyst film then functions as a robust, bifunctional, and switchable catalyst for both hydrogen production and water oxidation. To the best of our knowledge, such properties have never been previously reported for copper-based catalyst.

EXPERIMENTAL DETAILS

Materials. All chemicals were obtained from J&K Chemicals Co. or Aldrich and used without further purification unless otherwise noted. The 0.1 M potassium borate electrolyte solutions were prepared by mixing approximate volumes of 0.1 M KOH and 0.1 M H_3BO_3 with deionized water (Bluewater Industries; resistivity: 18 MΩ·cm). Phosphate solutions (0.1 M) were prepared by mixing approximate volumes of 0.1 M $KHPO_4$ and 0.1 M KH_2PO_4. The tris(2-pyridylmethyl)amine and bis(2-pyridylmethyl) amine ligands and copper complexes were synthesized according to the reported method.[44,75−79]

Electrochemical Methods. All electrochemical experiments were performed at room temperature and analyzed with a CHI602E Instrument Potentiostat (purchased from Shanghai ChenHua Instrument Co., Ltd.). The Ag/AgCl

DOI: 10.1021/cs501480s
ACS Catal. 2015, 5, 1530−1538

electrode (3 M KCl, 0.21 V vs NHE) was used as the reference electrode. Pt wire was used as the counter electrode and fluorine-doped tin oxide (FTO) electrode or glassy carbon (GC) electrode as the working electrodes. Bulk electrolysis was carried out at variable potentials without *iR* compensation. All potentials reported in this paper were measured versus an Ag/AgCl reference electrode.

Cyclic Voltammetry. A glassy carbon (GC) electrode and FTO were used as the working electrode to obtain cyclic voltammograms. Prior to experiments, the GC electrode was successively polished with 1, 0.3, and 0.05 μm Al_2O_3 powder and cleaned with deionized water three times, and the FTO electrodes were successively ultrasonicated in deionized water, ethanol, and deionized water for 5 min and dried in the air. All cyclic voltammograms were measured at 50 mV/s in 0.1 M potassium borate electrolytes containing a copper(II) complex. The CV scans were recorded in a range of 0 V ~ 1.50 V (vs Ag/AgCl). For the CV tests, there were *iR* compensations.

Bulk Electrolysis. The films depositions were performed at a controlled potential separately in a 0.1 M potassium borate (KBi) solution (pH = 9.2) and phosphate solution (pH = 7.0) containing 0.68 mM copper(II) complex. After a few hours of deposition, the films on FTO were washed with deionized water and acetone, dried in the air, and then transferred into a fresh KBi buffer solution containing no copper(II) complex for bulk electrolysis to study the catalytic activities of films.

Faradaic Efficiency. A fluorescence-based oxygen sensor (Ocean Optics) was used for quantitative detection of O_2. The experiment was performed in a gastight electrochemical cell. The solution was degassed by bubbling with high-purity N_2 for 20 min with vigorous stirring. The CuCat catalyst film deposited on FTO surface was used as the working electrode. The reference electrode was positioned several millimeters from the working electrode. The O_2 sensor on the FOXY probe, recorded at 2 s intervals, was converted into the partial pressure of O_2 in the headspace. After recording the partial pressure of O_2 for 30 min in the absence of an applied potential, electrolysis was initiated at +1.20 V without *iR* drop compensation.

Hydrogen Production Reaction. The hydrogen production experiments were performed in a gastight electrochemical cell, the solution was 0.1 M potassium borate solution at pH 9.2 with the H_2−CuCat-coated FTO as the working electrode obtained from **Cu-TPA.** Before the test, the exclusion of air by bubbling with high purity N_2 was performed for 20 min with vigorous stirring, at the applied potential −1.20 V. Hydrogen gas evolution was measured by gas chromatography (SP-6890, nitrogen as a carrier gas) with thermal conductivity detection (TCD).

Scanning Electron Microscopy (SEM) and Energy-Dispersive X-ray Analysis (EDX). SEM images and EDX spectra were obtained with a SIRION200 Schottky field emission scanning electron microscope (SFE-SEM) equipped with a Rontec EDX system. The detected samples were rinsed with deionized water and dried in the air and then coated with Pt to make the samples conductive before loading into the instrument. Images were obtained with an acceleration voltage of 5 kV and 10 kV.

X-ray Photoelectron Spectroscopy (XPS). The elemental composition of the catalysts on the top of FTO and the valence states of metal elements were probed with the ESCALAB 250 X-ray photoelectron spectroscopy (XPS) instrument. The survey scan and the high resolution Cu 2p spectra were obtained. The spectra are referenced to the C 1s peak (285.0 eV).

X-ray Diffraction (XRD, D/max-TTR III). The crystal phase analysis of the catalysts on the top of FTO after bulk electrolysis was measured by X-ray diffraction (XRD, D/max-TTR III) via graphite monochromatized Cu Kα radiation of 1.54178 Å, operating at 40 kV and 200 mA. The scanning rate was 5° min^{-1} from 10° to 70° in 2θ.

■ ASSOCIATED CONTENT

Supporting Information

The following file is available free of charge on the ACS Publications website at DOI: 10.1021/cs501480s.

Additional characterization data and figures, including CV scans, bulk electrolysis, SEM images, XPS data, and powder XRD data (PDF)

■ AUTHOR INFORMATION

Corresponding Author

*E-mail: dupingwu@ustc.edu.cn. Tel/Fax: 86-551-63606207.

Notes

The authors declare no competing financial interest.

■ ACKNOWLEDGMENTS

This work was financially supported by the National Natural Science Foundation of China (21271166, 21473170), the Fundamental Research Funds for the Central Universities, the Program for New Century Excellent Talents in University (NCET), and the Young Thousand Talents Program.

■ REFERENCES

(1) Gray, H. B. *Nat. Chem.* **2009**, *1*, 7.
(2) Lewis, N. S.; Nocera, D. G. *Proc. Natl. Acad. Sci. U.S.A.* **2006**, *103*, 15729−15735.
(3) Walter, M. G.; Warren, E. L.; McKone, J. R.; Boettcher, S. W.; Mi, Q. X.; Santori, E. A.; Lewis, N. S. *Chem. Rev.* **2010**, *110*, 6446−6473.
(4) Dresselhaus, M. S.; Thomas, I. L. *Nature* **2001**, *414*, 332−337.
(5) Armaroli, N.; Balzani, V. *Angew. Chem., Int. Ed.* **2006**, *46*, 52−66.
(6) Cook, T. R.; Dogutan, D. K.; Reece, S. Y.; Surendranath, Y.; Teets, T. S.; Nocera, D. G. *Chem. Rev.* **2010**, *110*, 6474−6502.
(7) Esswein, A. J.; Nocera, D. G. *Chem. Rev.* **2007**, *107*, 4022−4047.
(8) McEvoy, J. P.; Brudvig, G. W. *Chem. Rev.* **2006**, *106*, 4455−4483.
(9) Alstrum-Acevedo, J. H.; Brennaman, M. K.; Meyer, T. J. *Inorg. Chem.* **2005**, *44*, 6802−6827.
(10) Grätzel, M. *Acc. Chem. Res.* **1981**, *14*, 376−384.
(11) Duan, L.; Bozoglian, F.; Mandal, S.; Stewart, B.; Privalov, T.; Llobet, A.; Sun, L. *Nat. Chem.* **2012**, *4*, 418−423.
(12) Blakemore, J. D.; Schley, N. D.; Balcells, D.; Hull, J. F.; Olack, G. W.; Incarvito, C. D.; Eisenstein, O.; Brudvig, G. W.; Crabtree, R. H. *J. Am. Chem. Soc.* **2010**, *132*, 16017−16029.
(13) Blakemore, J. D.; Mara, M. W.; Kushner-Lenhoff, M. N.; Schley, N. D.; Konezny, S. J.; Rivalta, I.; Negre, C. F. A.; Snoeberger, R. C.; Kokhan, O.; Huang, J.; Stickrath, A.; Tran, L. A.; Parr, M. L.; Chen, L. X.; Tiede, D. M.; Batista, V. S.; Crabtree, R. H.; Brudvig, G. W. *Inorg. Chem.* **2013**, *52*, 1860−1871.
(14) Lalrempuia, R.; McDaniel, N. D.; Muller-Bunz, H.; Bernhard, S.; Albrecht, M. *Angew. Chem., Int. Ed.* **2010**, *49*, 9765−9768.
(15) McDaniel, N. D.; Coughlin, F. J.; Tinker, L. L.; Bernhard, S. *J. Am. Chem. Soc.* **2008**, *130*, 210−217.
(16) Du, P.; Eisenberg, R. *Energy Environ. Sci.* **2012**, *5*, 6012−6021.
(17) Fukuzumi, S.; Hong, D. C.; Yamada, Y. *J. Phys. Chem. Lett.* **2013**, *4*, 3458−3467.
(18) Fukuzumi, S.; Hong, D. C. *Eur. J. Inorg. Chem.* **2014**, 645−659.
(19) Kanan, M. W.; Nocera, D. G. *Science* **2008**, *321*, 1072−1075.
(20) Nocera, D. G. *Acc. Chem. Res.* **2012**, *45*, 767−776.

DOI: 10.1021/cs501480s
ACS Catal. 2015, 5, 1530−1538

(21) Artero, V.; Chavarot-Kerlidou, M.; Fontecave, M. *Angew. Chem., Int. Ed.* **2011**, *50*, 7238−7266.
(22) Du, P.; Knowles, K.; Eisenberg, R. *J. Am. Chem. Soc.* **2008**, *130*, 12576−12577.
(23) Han, A.; Wu, H.; Sun, Z.; Jia, H.; Yan, Z.; Ma, H.; Liu, X.; Du, P. *ACS Appl. Mater. Interfaces* **2014**, *6*, 10929−10934.
(24) Hong, D.; Jung, J.; Park, J.; Yamada, Y.; Suenobu, T.; Lee, Y.-M.; Nam, W.; Fukuzumi, S. *Energy Environ. Sci.* **2012**, *5*, 7606−7616.
(25) Bediako, D. K.; Lassalle-Kaiser, B.; Surendranath, Y.; Yano, J.; Yachandra, V. K.; Nocera, D. G. *J. Am. Chem. Soc.* **2012**, *134*, 6801−6809.
(26) Dinca, M.; Surendranath, Y.; Nocera, D. G. *Proc. Natl. Acad. Sci. U. S. A.* **2010**, *107*, 10337−10341.
(27) Yu, X.; Xu, P.; Hua, T.; Han, A.; Liu, X.; Wu, H.; Du, P. *Int. J. Hydrogen Energy* **2014**, *39*, 10467−10475.
(28) Hong, D. C.; Yamada, Y.; Nagatomi, T.; Takai, Y.; Fukuzumi, S. *J. Am. Chem. Soc.* **2012**, *134*, 19572−19575.
(29) Fillol, J. L.; Codola, Z.; Garcia-Bosch, I.; Gomez, L.; Pla, J. J.; Costas, M. *Nat. Chem.* **2011**, *3*, 807−813.
(30) Ellis, W. C.; McDaniel, N. D.; Bernhard, S.; Collins, T. J. *J. Am. Chem. Soc.* **2010**, *132*, 10990−10991.
(31) Surendranath, Y.; Dinca, M.; Nocera, D. G. *J. Am. Chem. Soc.* **2008**, *131*, 2615−2620.
(32) Kanan, M. W.; Surendranath, Y.; Nocera, D. G. *Chem. Soc. Rev.* **2009**, *38*, 109−114.
(33) Huang, Z.; Luo, Z.; Geletii, Y. V.; Vickers, J. W.; Yin, Q.; Wu, D.; Hou, Y.; Ding, Y.; Song, J.; Musaev, D. G.; Hill, C. L.; Lian, T. *J. Am. Chem. Soc.* **2011**, *133*, 2068−2071.
(34) Yin, Q.; Tan, J. M.; Besson, C.; Geletii, Y. V.; Musaev, D. G.; Kuznetsov, A. E.; Luo, Z.; Hardcastle, K. I.; Hill, C. L. *Science* **2010**, *328*, 342−345.
(35) Liang, Y.; Li, Y.; Wang, H.; Zhou, J.; Wang, J.; Regier, T.; Dai, H. *Nat. Mater.* **2011**, *10*, 780−786.
(36) Jiao, F.; Frei, H. *Angew. Chem., Int. Ed.* **2009**, *48*, 1841−1844.
(37) Hinnemann, B.; Moses, P. G.; Bonde, J.; Jørgensen, K. P.; Nielsen, J. H.; Horch, S.; Chorkendorff, I.; Nørskov, J. K. *J. Am. Chem. Soc.* **2005**, *127*, 5308−5309.
(38) Eckenhoff, W. T.; McNamara, W. R.; Du, P.; Eisenberg, R. *Biochim. Biophys. Acta, Bioenerg.* **2013**, *1827*, 958−973.
(39) Dubois, M. R.; Dubois, D. L. *Acc. Chem. Res.* **2009**, *42*, 1974−1982.
(40) Helm, M. L.; Stewart, M. P.; Bullock, R. M.; DuBois, M. R.; DuBois, D. L. *Science* **2011**, *333*, 863−866.
(41) Cobo, S.; Heidkamp, J.; Jacques, P. A.; Fize, J.; Fourmond, V.; Guetaz, L.; Jousselme, B.; Ivanova, V.; Dau, H.; Palacin, S.; Fontecave, M.; Artero, V. *Nat. Mater.* **2012**, *11*, 802−807.
(42) He, C.; Wu, X.; He, Z. *J. Phys. Chem. C* **2014**, *118*, 4578−4584.
(43) Yu, X.; Hua, T.; Liu, X.; Yan, Z.; Xu, P.; Du, P. *ACS Appl. Mater. Interfaces* **2014**, *6*, 15395−15402.
(44) Lewis, E. A.; Tolman, W. B. *Chem. Rev.* **2004**, *104*, 1047−1076.
(45) Mirica, L. M.; X, O.; Stack, T. D. P. *Chem. Rev.* **2004**, *104*, 1013−1045.
(46) Kang, P.; Bobyr, E.; Dustman, J.; Hodgson, K. O.; Hedman, B.; Solomon, E. I.; Stack, T. D. P. *Inorg. Chem.* **2010**, *49*, 11030−11038.
(47) Taki, M.; Itoh, S.; Fukuzumi, S. *J. Am. Chem. Soc.* **2001**, *123*, 6203−6204.
(48) Cramer, C. J.; Tolman, W. B. *Acc. Chem. Res.* **2007**, *40*, 601−608.
(49) Barnett, S. M.; Goldberg, K. I.; Mayer, J. M. *Nat. Chem.* **2012**, *4*, 498−502.
(50) Chen, Z. F.; Meyer, T. J. *Angew. Chem., Int. Ed.* **2013**, *52*, 700−703.
(51) Zhang, M. T.; Chen, Z. F.; Kang, P.; Meyer, T. J. *J. Am. Chem. Soc.* **2013**, *135*, 2048−2051.
(52) Zhang, T.; Wang, C.; Liu, S.; Wang, J.-L.; Lin, W. *J. Am. Chem. Soc.* **2014**, *136*, 273−281.
(53) Jahan, M.; Liu, Z.; Loh, K. P. *Adv. Funct. Mater.* **2013**, *23*, 5363−5372.
(54) Cao, J. P.; Fang, T.; Fu, L. Z.; Zhou, L. L.; Zhan, S. Z. *Int. J. Hydrogen Energy* **2014**, *39*, 13972−13978.
(55) Cao, J. P.; Fang, T.; Wang, Z. Q.; Ren, Y. W.; Zhan, S. Z. *J. Mol. Catal. A: Chem.* **2014**, *391*, 191−197.
(56) Chen, Z. F.; Kang, P.; Zhang, M. T.; Stoner, B. R.; Meyer, T. J. *Energy Environ. Sci.* **2013**, *6*, 813−817.
(57) Liu, X.; Jia, H.; Sun, Z.; Chen, H.; Xu, P.; Du, P. *Electrochem. Commun.* **2014**, *46*, 1−4.
(58) Zhao, W.; Fu, W.; Yang, H.; Tian, C.; Li, M.; Li, Y.; Zhang, L.; Sui, Y.; Zhou, X.; Chen, H.; Zou, G. *CrystEngComm* **2011**, *13*, 2871−2877.
(59) Poulston, S.; Parlett, P. M.; Stone, P.; Bowker, M. *Surf. Interface Anal.* **1996**, *24*, 811−820.
(60) Yu, J.; Hai, Y.; Jaroniec, M. *J. Colloid Interface Sci.* **2011**, *35*, 223−228.
(61) Chen, S.; Duan, J. J.; Ran, J. R.; Jaroniec, M.; Qiao, S. Z. *Energy Environ. Sci.* **2013**, *6*, 3693−3699.
(62) Mcintyre, N. S.; Cook, M. G. *Anal. Chem.* **1975**, *47*, 2208−2213.
(63) Deroubaix, G.; Marcus, P. *Surf. Interface Anal.* **1992**, *18*, 39−46.
(64) Xu, S.; Ng, J.; Du, A. J. o.; Liu, J.; Sun, D. D. *Int. J. Hydrogen Energy* **2011**, *36*, 6538−6545.
(65) McIntyre, N. S.; Sunder, S.; Shoesmith, D. W.; Stanchell, F. W. *J. Vac. Sci. Technol.* **1981**, *18*, 714−721.
(66) Kishi, K.; Ikeda, S. *Chem. Lett.* **1972**, 245−246.
(67) Asami, K.; Hashimoto, K.; Shimodaira, S. *Corros. Sci.* **1978**, *18*, 151−160.
(68) Pinkas, J.; Huffman, J. C.; Baxter, D. V.; Chisholm, M. H.; Caulton, K. G. *Chem. Mater.* **1995**, *7*, 1589−1596.
(69) Lalitha, K.; Sadanandam, G.; Kumari, V. D.; Subrahmanyam, M.; Sreedhar, B.; Hebalkar, N. Y. *J. Phys. Chem. C* **2010**, *114*, 22181−22189.
(70) Paracchino, A.; Laporte, V.; Sivula, K.; Gratzel, M.; Thimsen, E. *Nat. Mater.* **2011**, *10*, 456−461.
(71) Duan, L.; Tong, L.; Xu, Y.; Sun, L. *Energy Environ. Sci.* **2011**, *4*, 3296−3313.
(72) Nian, J.; Hu, C.; Teng, H. *Int. J. Hydrogen Energy* **2008**, *33*, 2897−2903.
(73) Paracchino, A.; Brauer, J. C.; Moser, J. E.; Thimsen, E.; Graetzel, M. *J. Phys. Chem. C* **2012**, *116*, 7341−7350.
(74) Siripala, W.; Ivanovskaya, A.; Jaramillo, T. F.; Baeck, S. H.; McFarland, E. W. *Sol. Energy Mater. Sol. Cells* **2003**, *77*, 229−237.
(75) Hajiashrafi, T.; Kharat, A. N.; Love, J. A.; Patrick, B. O. *Polyhedron* **2013**, *60*, 30−38.
(76) Jacobson, R. R.; Tyeklar, Z.; Karlin, K. D.; Zubieta, J. *Inorg. Chem.* **1991**, *30*, 2035−2040.
(77) Nagao, H.; Komeda, N.; Mukaida, M.; Suzuki, M.; Tanaka, K. *Inorg. Chem.* **1996**, *35*, 6809−6815.
(78) Lucas, H. R.; Li, L.; Sarjeant, A. A. N.; Vance, M. A.; Solomon, E. I.; Karlin, K. D. *J. Am. Chem. Soc.* **2009**, *131*, 3230−3245.
(79) Rojas, D.; Garcia, A. M.; Vega, A.; Moreno, Y.; Venegas-Yazigi, D.; Garland, M. T.; Manzur, J. *Inorg. Chem.* **2004**, *43*, 6324−6330.

DOI: 10.1021/cs501480s
ACS Catal. 2015, 5, 1530−1538